Oecologia (2014) 176:703–714
DOI 10.1007/s00442-014-3059-7

METHODS

Instantaneous-to-daily GPP upscaling schemes based on a coupled photosynthesis-stomatal conductance model: correcting the overestimation of GPP by directly using daily average meteorological inputs

Fumin Wang · Alemu Gonsamo · Jing M. Chen · T. Andrew Black · Bin Zhou

Received: 27 July 2013 / Accepted: 19 August 2014 / Published online: 3 September 2014

Abstract Daily canopy photosynthesis is usually temporally upscaled from instantaneous (i.e., seconds) photosynthesis rate. The nonlinear response of photosynthesis to meteorological variables makes the temporal scaling a significant challenge. In this study, two temporal upscaling schemes of daily photosynthesis, the integrated daily model (IDM) and the segmented daily model (SDM), are presented by considering the diurnal variations of meteorological variables based on a coupled photosynthesis-stomatal conductance model. The two models, as well as a simple average daily model (SADM) with daily average meteorological inputs, were validated using the tower-derived gross primary production (GPP) to assess their abilities in simulating daily photosynthesis. The results showed IDM closely followed the seasonal trend of the tower-derived GPP with an average RMSE of 1.63 g C m^{-2} day^{-1}, and an average Nash–Sutcliffe model efficiency coefficient (*E*) of 0.87. SDM performed similarly to IDM in GPP simulation but decreased the computation time by >66 %. SADM overestimated daily GPP by about 15 % during the growing season compared to IDM. Both IDM and SDM greatly decreased the overestimation by SADM, and improved the simulation of daily GPP by reducing the RMSE by 34 and 30 %, respectively. The results indicated that IDM and SDM are useful temporal upscaling approaches, and both are superior to SADM in daily GPP simulation because they take into account the diurnally varying responses of photosynthesis to meteorological variables. SDM is computationally more efficient, and therefore more suitable for long-term and large-scale GPP simulations.

Keywords Gross primary production · Temporal scaling · Integrated daily model · Segmented daily model

Communicated by Russell Monson.

Electronic supplementary material The online version of this article (doi:10.1007/s00442-014-3059-7) contains supplementary material, which is available to authorized users.

F. Wang (✉)
Institute of Hydrology and Water Resources, Zhejiang University, Zijingang Campus, Hangzhou 310058, China
e-mail: wfmwfmwfmwfm@163.com

A. Gonsamo · J. M. Chen
Department of Geography and Program in Planning, University of Toronto, Toronto M5S 3G3, ON, Canada

T. A. Black
Faculty of Land and Food Systems, University of BC, 2357 Main Mall, Vancouver, BC V6T 1Z4, Canada

B. Zhou
Institute of Remote Sensing and Earth Sciences, Hangzhou Normal University, Hangzhou, China

Introduction

Gross primary production (GPP), or gross ecosystem photosynthesis, is a key component of the carbon balance of terrestrial ecosystems. GPP at long time scales up to years, decades and centuries, and at large spatial scales up to regions and the globe, are usually needed in evaluating terrestrial and global carbon dynamics influenced by climate change and human activities (Pan et al. 2009). Process-based models provide useful exploratory and predictive tools for simulating GPP with increasing computational efficiency for large-scale, multi-year simulations. Among process-based models, daily canopy models, e.g., Forest-BGC (Running and Coughlan 1988), daily BEPS (Liu et al. 1997), BGC++ (Hunt et al. 1999), daily DNDC (Li

2000), BIOME-BGC (Thornton et al. 2002), EPIC (Izaurralde et al. 2006), and DLEM (Tian et al. 2010), are widely used at regional and global scales because daily meteorological inputs to these models are easier to obtain than hourly meteorological data, especially for historical GPP simulations.

The ideal way to accurately obtain the daily GPP is to integrate the instantaneous (i.e., seconds) leaf-level processes over space and time (Mäkelä et al. 2006). However, to date, this is still a challenging task due to the intricate nonlinear relationships between photosynthesis and the controlling environmental, structural and nutritional parameters varying with time and depth in the canopy (Chen et al. 1999, 2009; Lim and Roderick 2012), in spite the fact that the instantaneous response of leaf photosynthesis to environmental variables is well understood (Farquhar et al. 1980). Some alternative methods have been developed for addressing the spatiotemporal upscaling. As for spatial upscaling from leaf level to canopy level, the big-leaf model was initially proposed. After that, the separation of sunlit and shaded leaves with two-layer or multilayer canopy models was made for spatial upscaling of canopy photosynthesis (Chen et al. 1999; Wang and Leuning 1998; Bonan et al. 2012).

Temporal upscaling methods have also been developed and can be classified into two broad categories. Firstly, daily integral of Farquhar's model (Farquhar et al. 1980) with respect to stomatal conductance rather than time (Chen et al. 1999; Jin et al. 2003). These models were developed based on the assumption that the temperature-dependent parameters and the photosynthetic photon flux density (PPFD)-dependent parameter (J) in Farquhar's model (Farquhar et al. 1980) change approximately linearly with meteorological variables during the day. These conditions are usually not fulfilled, especially for J which is remarkably nonlinear in response to PPFD during daytime. Moreover, another possible weakness is the use of the Jarvis's empirical (Jarvis 1976) multiplicative model of stomatal conductance in contrast to the more mechanistic Leuning model (Leuning 1995). Secondly, a simple average daily model based on the coupling of the Farquhar (Farquhar et al. 1980) with the Ball-Berry (Ball 1988) or Leuning models. In this model, the instantaneous photosynthesis rate is first derived by iteratively solving coupled equations describing photosynthesis and stomatal conductance for steady-state conditions (Leuning 1990; Sellers et al. 1992) or by analytically solving a cubic equation (Baldocchi 1994). Following that, the instantaneous photosynthesis rate is multiplied by the length of daytime to obtain daily photosynthesis. In this way, despite the use of a mechanistic model for stomatal conductance, the diurnal variations of meteorological parameters are not considered, leading to overestimation of photosynthesis due to the possible increase in light use efficiency when the mean incident PPFD is used for the day (Chen et al. 1999). The overestimations are usually compensated by adjustments of other model parameters such as V_{cmax}, which may partly explain why some models use very different V_{cmax} values which are usually smaller than observed values (Bonan et al. 2012).

The second category of daily canopy photosynthesis models has been widely used. Over the years, less attention has been given to the effect of ignoring diurnal variations in meteorological variables on daily GPP and the corresponding overestimation of GPP caused by ignoring the non-linearity of many underlying processes. Therefore, the objectives of this study are: (1) to test the simple average daily model which uses daily average meteorological data inputs, and (2) to develop new schemes for temporal upscaling of photosynthesis from instantaneous to daily values. The emphasis is put on the removal of the overestimation due to the use of the daily mean meteorological data. In the meantime, we also introduce the improved Ball-Berry model, Leuning's (1995) model, into daily canopy photosynthesis simulation. The use of Leuning's model will not only improve the parameterization of the physiological mechanism but also facilitate the calculation of evapotranspiration by introducing the modeled stomatal conductance into the Penman–Monteith equation which is considered an accurate method to estimate evapotranspiration. In this study, first, an integrated daily model based on a numerical solution is presented using the diurnal pattern of meteorological variables, and then a segmented daily model is developed for the calculation of daily canopy photosynthesis. The segmented daily model will be evaluated for its computational efficiency and accuracy for calculating daily canopy photosynthesis.

Materials and methods

Description of study sites and data

Two forest sites with CO_2 eddy-covariance (EC) and meteorological measurements were selected for this study. Site descriptions are given in Table 1. One is the Old Aspen site (SK-OA), located near the south end of the Prince Albert National Park. The canopy at this site consists of a trembling aspen overstorey with average tree height of 21 m and a dense hazelnut understorey with canopy height between 1 and 3 m. The leaf area index (LAI) values show moderate inter-annual variability for the aspen overstorey [mean ± standard deviation (SD) of 2.44 ± 0.30] and the hazelnut understory (mean ± SD of 1.98 ± 0.44) during 1994–2003 (Barr et al. 2004). The soil is an Orthic Gray Luvisol with an 8- to 10-cm-deep surface organic layer overlying a loam to sandy clay loam mineral soil.

Table 1 Description of the study sites

Description	Site	
	SK-OA	BC-DF49
Latitude (°N)	53.62889	49.86883
Longitude (°W)	106.19779	125.33508
Vegetation type	Deciduous boreal forest	Coniferous temperate forest
Dominant species	Mature aspen with dense hazel understorey	Douglas-fir, western red cedar, sparse understorey
Stand age (years)	89	63
Elevation (m)	601	300
Soil texture	Sandy clay loam	Gravelly sandy loam
Mean annual Temperature (°C)	0.5	7.9
Mean annual precipitation (mm)	406	1,179
Reference	Barr et al. (2004)	Jassal et al. (2009)

SK-OA the Old Aspen site, *BC-DF49* the Douglas-fir forest site

The other site is Douglas-fir forest site (BC-DF49), located 10 km Southwest of Campbell River on the east coast of Vancouver Island, BC, Canada, at an elevation of 300 m above sea level. The forest consists of 80 % Douglas-fir, 17 % western red cedar, and 3 % western hemlock. The stand density is 1,100 stems ha^{-1}, with tree height ranging between 30 and 35 m (Chen et al. 2006). The understory is sparse, mainly consisting of salal, Oregon grape, vanilla-leaf deer foot, and various ferns and mosses. The average LAI value for the site is about 6.1 (Chen et al. 2009). The soil is a Humo-Ferric Podzol with a gravelly sandy loam texture and a surface organic layer averaging 3 cm, but ranging from 1 to 10 cm in depth.

Flux and meteorological data at these two sites were obtained from the Canadian Carbon Program (CCP) formerly known as Fluxnet-Canada archive (http://www.fluxnet-canada.ca). At both sites, the standard meteorological variables and the fluxes of CO_2, water vapor and sensible heat were measured half-hourly using sensors mounted on towers as part of the CCP. Net ecosystem exchange (NEE) was determined as the sum of half-hourly EC flux of CO_2 and the rate of change in CO_2 storage in the air column between ground and EC-measurement level. Net ecosystem productivity (NEP) was calculated as NEP = −NEE, and GPP was calculated as the sum of daytime NEP and daytime ecosystem respiration calculated using the relationship between nighttime CO_2 flux (nighttime ecosystem respiration) and shallow soil temperature. The CO_2 fluxes had been gap-filled using a flexible moving window approach developed for the CCP (Barr et al. 2004).

Temporal upscaling schemes

Three temporal upscaling schemes for leaf-level daily photosynthesis calculation based on improved instantaneous photosynthesis model developed by Baldocchi (1994) were adopted in this study.

A brief introduction of instantaneous photosynthesis model

Since the instantaneous photosynthesis model is the basis and premise of daily ecosystem process models, it will be briefly introduced here. An improved instantaneous photosynthesis model (Baldocchi 1994), hereafter referred to as the Baldocchi model, is used in this study. The improved Baldocchi model couples Farquhar's model (Farquhar et al. 1980) with Leuning's model (Leuning 1995) rather than the Ball-Berry stomatal conductance model (Ball 1988) because vapor pressure deficit can better describe the response of stomatal conductance to humidity than relative humidity (Leuning 1995; Oren et al. 1999; Katul et al. 2009). The improved Baldocchi model is derived from solving a cubic equation and obtaining the appropriate root as the resultant net photosynthesis rate. Root three (Eqs. 1a–1d) is usually correct for a wide range of environmental conditions commonly encountered in the field (Baldocchi 1994). This root is expressed as follows:

$$A_{\text{net}} = -2\sqrt{\frac{p^2-3q}{9}}\cos\left(\frac{\arccos\left(\frac{2p^3-9pq+27r}{2\sqrt{(p^2-3q)^3}}\right)+4\pi}{3}\right)-\frac{p}{3} \quad (1a)$$

$$p = \frac{f\beta + b\theta' - a\alpha + f\alpha R_{\text{d}}}{f\alpha} \quad (1b)$$

$$q = \frac{f\gamma + \frac{b\gamma}{C_{\text{a}}} - a\beta + ad\theta' + fR_{\text{d}}\beta + R_{\text{d}}b\theta'}{f\alpha} \quad (1c)$$

$$r = \frac{-a\gamma + \frac{ad\gamma}{C_{\text{a}}} + fR_{\text{d}}\gamma + \frac{R_{\text{d}}b\gamma}{C_{\text{a}}}}{f\alpha} \quad (1d)$$

and $\alpha = 1 + \frac{b'}{g_b} - mh_s$, $\beta = C_a(g_b mh_s - 2b' - g_b)$, $\gamma = C_a^2 b' g_b$, $\theta' = g_b mh_s - b'$,where A_{net} is the net photosynthesis rate, R_d is the daytime dark respiration of the leaf, C_a is the CO_2 concentration of the air outside the leaf boundary layer, g_b is the leaf boundary layer conductance, m is a plant species-dependent coefficient, h_s is the humidity factor at the leaf surface ($h_s = 1/(1 + D_s/D_0)$, where D_s is the vapor pressure deficit (VPD) at the leaf surface, D_0 is an empirical parameter.), and b' is the residual conductance which is a small value due to leaf dark respiration. The parameters a, b, d, and f are from Farquhar's model which can be written in the algebraic form: $A_{net} = \frac{aC_i - ad}{fC_i + b} - R_d$. In the improved Baldocchi model, the meteorological variables, PAR, air temperature and VPD, etc., are the final input model parameters.

Instantaneous-to-daily temporal upscaling schemes

Integrated daily model (IDM) Solar radiation, temperature and relative humidity are the critical variables that drive biological systems and are of fundamental importance in process-based ecosystem models. In order to integrate the instantaneous photosynthesis rate over time, the diurnal courses of these variables are needed for the calculation of daily GPP. Since these meteorological variables vary approximately sinusoidally during the daytime, it is feasible to describe most of this variation using a sine or cosine function.

The diurnal variation of global radiation can be described using a simple sine function (Kimball and Bellamy 1986):

$$R_t = R_{noon} \sin\left[\frac{\pi(t - t_{rise})}{t_{set} - t_{rise}}\right] = \frac{\pi R_{daily}}{2\ \text{day length}} \sin\left[\frac{\pi(t - t_{rise})}{t_{set} - t_{rise}}\right] \quad (2)$$

where R_t is the instantaneous global solar radiation (W m^{-2}) at solar time t, R_{noon} is the global solar radiation at solar noon, $t_{set} - t_{rise}$ is the day length (s), and R_{daily} is the daily total solar radiation.

The air temperature and relative humidity during the daylight hours can be described by the following equations (Reicosky et al. 1989):

$$T_t = T_{min} + (T_{max} - T_{min}) \sin\left[\frac{\pi(t - t_{rise})}{t_{set} - t_{rise} + 2a}\right] \quad (3)$$

$$HR_t = HR_{max} - (HR_{max} - HR_{min}) \sin\left[\frac{\pi(t - t_{rise})}{t_{set} - t_{rise} + 2a}\right] \quad (4)$$

where T_t, HR_t are air temperature and relative humidity (which would be converted to VPD in photosynthesis models) at time t in seconds (s), T_{max} and T_{min} are daily maximum and minimum air temperature, HR_{max} and HR_{min} $T_{min}$are daily maximum and minimum relative humidity, t_{rise} is the time of sunrise, t_{set} is the time of sunset, a is the time difference (lag) between the time of T_{max} and the solar noon, here assumed to be 2 h. The times for sunrise and sunset can be determined by the day of the year and the latitude of a site. If the time lag of the maximum air temperature after solar noon is not considered, the daily course of the air temperature and relative humidity can be expressed using Eqs. 3 and 4 with a set to zero. The simulation results from Eqs. 3 and 4 were validated by measured data (Online Resource 1). The R^2 values between the modeled and measured solar radiation, air temperature, and VPD are 0.91, 0.98 and 0.91 for the SK-OA site and 0.93, 0.98 and 0.87 for the BC-DF49 site, respectively.

Since the three meteorological inputs can be simulated using their daily values, daily total photosynthesis can be obtained by integrating the instantaneous photosynthesis rate with respect to time from sunrise to sunset. The daily GPP is thus calculated using the following equation:

$$\begin{aligned} GPP_{daily} &= \int_{t_{rise}}^{t_{set}} A_{net}\,dt \\ &= \int_{t_{rise}}^{t_{set}} \left(-2\sqrt{\frac{p^2 - 3q}{9}} \times \cos\left(\frac{\arccos\left(\frac{2p^3 - 9pq + 27r}{2\sqrt{(p^2 - 3q)^3}}\right) + 4\pi}{3}\right) - \frac{p}{3}\right) dt \end{aligned} \quad (5)$$

where p, q, r are the same parameters as in Eqs. 1a–1d. In theory, an analytic expression for calculating the daily GPP could be obtained if the symbolic integration of Eq. 5 were possible. However, it is difficult to obtain an analytical solution due to the complexity of the Eq. 5 resulting from the nonlinear response of GPP to environmental factors and the interactions among meteorological variables. So, numerical integration is made to obtain the daily GPP in the study, where hourly GPP values are computed with the values of hourly meteorological input variables obtained from the models (Eqs. 2–4) and summed into daily values.

Segmented daily model (SDM) Although numerical integration mentioned above is numerically stable and no additional parameters are introduced during the diurnal numerical integration, considerable computation time is needed. In order to avoid the excessive computational demand through numerical integration and yet to consider the effects of the

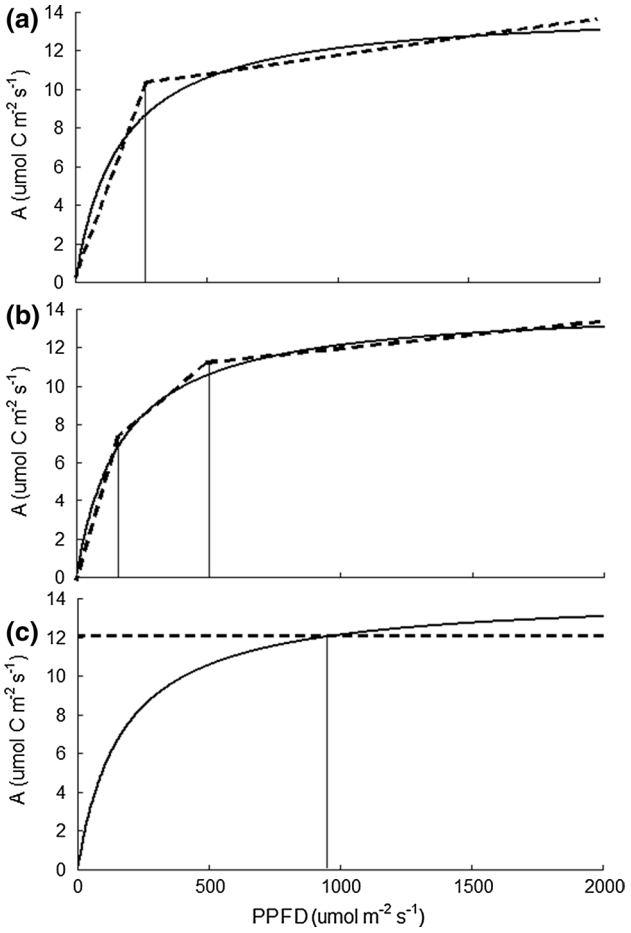

Fig. 1 Schematic diagram of **a** two-segment, **b** three-segment and **c** simple average daily models for daily photosynthesis calculation

diurnal variation pattern of meteorological variables on photosynthesis, a segmented daily model with improved computational efficiency on the basis of the instantaneous photosynthesis model is developed for the photosynthesis calculation at a daily time step after carefully examining the response patterns of GPP to solar radiation (Fig. 1a, b). The SDM can be expressed as follows:

$$\mathrm{GPP_{daily}} = 2 \times \sum_{i=1}^{n} \left(A_{\mathrm{net},i} \times D_{t_i}\right) \tag{6}$$

where $A_{\mathrm{net},i}$ is the instantaneous photosynthesis rate in a time interval, D_{t_i}(s), and n is the number of time intervals between sunrise and solar noon. In the SDM model, the meteorological data are assumed to be symmetrical following a sine function with a peak at solar noon although there is a time lag for temperature. The effect of the time lag will be analyzed in the latter section, and therefore, the photosynthesis in the morning equals to that in the afternoon. Therefore, daily photosynthesis is obtained by multiplying the photosynthesis in the morning by 2.

The assumption behind SDM is that since the response of GPP to the radiation during the whole day is nonlinear, the response of GPP to radiation in a relatively small time period can be seen as being linear. Figure 1a, b is the schematic diagram for two-segment and three-segment daily models which shows that the three-segment daily model (SDM-3) coincides well with the continuous photosynthesis rate compared to the two-segment daily model (SDM-2). However the difference between them is relatively small compared with the daily total GPP. Therefore, we chose SDM-2 for daily total GPP calculation in this study. The SDM-2 can be expressed in the form:

$$\mathrm{GPP_{daily}} = 2 \times \left(A_{\mathrm{net},1} \times D_{t_1} + A_{\mathrm{net},2} \times D_{t_2}\right) \tag{7}$$

where $A_{\mathrm{net},1}$ and $A_{\mathrm{net},2}$ are the instantaneous photosynthesis rate at solar time t_1 and t_2, respectively. D_{t_1} and D_{t_2} are the time interval length.

In order to obtain the values of t_1 and t_2, the time of day corresponding to average daily global solar radiation, expressed as the time t_0, must be determined first. The procedure for deriving the time, t_0, is given as follows:

$$\begin{aligned} \mathrm{R_{daily}} &= R_{\mathrm{noon}} \int_{t_{\mathrm{rise}}}^{t_{\mathrm{set}}} \sin\left[\frac{\pi(t - t_{\mathrm{rise}})}{t_{\mathrm{set}} - t_{\mathrm{rise}}}\right] \\ \mathrm{d}t &= \frac{2R_{\mathrm{noon}}(t_{\mathrm{set}} - t_{\mathrm{rise}})}{\pi} = f(t_0) \times (t_{\mathrm{set}} - t_{\mathrm{rise}}) \\ &= R_{\mathrm{noon}} \sin\left[\frac{\pi(t_0 - t_{\mathrm{rise}})}{t_{\mathrm{set}} - t_{\mathrm{rise}}}\right] \times (t_{\mathrm{set}} - t_{\mathrm{rise}}) \end{aligned} \tag{8}$$

$$t_0 = \frac{t_{\mathrm{set}} - t_{\mathrm{rise}}}{\pi} \arcsin\left(\frac{2}{\pi}\right) + t_{\mathrm{rise}} \tag{9}$$

With t_0, we can derive expressions for t_1 and t_2.

$$t_1 = \frac{(t_{\mathrm{set}} - t_{\mathrm{rise}})\arcsin\left(\frac{2}{\pi}\right)}{2\pi} + t_{\mathrm{rise}} \tag{10}$$

$$t_2 = \frac{t_{\mathrm{set}} - t_{\mathrm{rise}}}{4} + \frac{t_{\mathrm{set}} - t_{\mathrm{rise}}}{2\pi} \arcsin\left(\frac{2}{\pi}\right) + t_{\mathrm{rise}} \tag{11}$$

The meteorological variables at solar time t_1, t_2 are taken from sinusoidal models (Eqs. 10, 11) and the instantaneous photosynthesis rates, $A_{\mathrm{net},1}$ and $A_{\mathrm{net},2}$, are calculated by Eq. 1a.

The $D_{t_1}$and D_{t_2} are derived by following equations:

$$D_{t_1} = \frac{t_{\mathrm{set}} - t_{\mathrm{rise}}}{\pi} \arcsin\left(\frac{2}{\pi}\right) \tag{12}$$

$$D_{t_2} = \frac{t_{\mathrm{set}} - t_{\mathrm{rise}}}{2} - \frac{t_{\mathrm{set}} - t_{\mathrm{rise}}}{\pi} \arcsin\left(\frac{2}{\pi}\right) \tag{13}$$

Table 2 Key parameters used for the two study sites

Description	Symbol	Unit	SK-OA	BC-DF49	References
Maximum carboxylation capacity,	V_{cmax}	$\mu mol\ m^{-2}\ s^{-1}$	60	54	Groenendijk et al. (2011)
Nitrogen content at the top of the canopy	N_0	$g\ m^{-2}$	1.74	3.1	Kattge et al. (2009)
Relative change of V_{cmax} with nitrogen	χ_n	$m^2\ g^{-1}$	0.59	0.33	Kattge et al. (2009)
Stomatal conductance coefficient	m		8	8	Ball (1988), Medlyn et al. (1999)
Residual conductance	b'	$mol\ m^{-2}\ s^{-1}$	0.0011	0.0011	Ball (1988), Leuning (1995)

Simple average daily model (SADM) In order to compare IDM and SDM with the temporal upscaling scheme without considering the diurnal variations of meteorological variables, the simple average daily model (SADM) is also presented here (Fig. 1c). The daily total or average values of meteorological variables are used as inputs for SADM without considering the diurnal variation of these variables. In the model, the total solar radiation is averaged by the daylength (i.e., length of daytime). The maximum and minimum temperatures are used to calculate the daytime average temperature using $0.212 \times (T_{max} - (T_{max} + T_{min})/2) + (T_{max} + T_{min})/2$. The daily gross primary production (GPP_{daily}) is therefore calculated as:

$$GPP_{daily} = A_{net} \times \text{daylength} \tag{14}$$

where A_{net} is the instantaneous net photosynthesis rate calculated using the daily total/average meteorological variables. The daylength is the astronomical day length.

Daily GPP simulation models based on temporal upscaling schemes

The above three temporal uspcaling schemes were integrated into the framework of Boreal Ecosystem Productivity Simulator (BEPS) (Liu et al. 1997) to construct new daily BEPS models to calculate canopy-level GPP. In the model framework of BEPS, the canopy is stratified into sunlit and shaded leaf groups using the formulation of Chen et al. (1999), and the canopy-level GPP (GPP_{canopy}) is the sum of the total GPP of these two leaf groups:

$$\begin{aligned} GPP_{canopy} = {} & GPP_{sunlit} \times LAI_{sunlit} \\ & + GPP_{shaded} \times LAI_{shaded} \end{aligned} \tag{15}$$

where the subscripts "sunlit" and "shaded" denote the sunlit and shaded components of GPP and LAI. The GPP_{sunlit} and GPP_{shaded} are calculated using BEPS by integrating the three temporal uspcaling schemes. The key parameters used for the two sites are given in Table 2.

Model evaluation

Half-hourly eddy-covariance measurements of CO_2 fluxes made at BC-DF49 and SK-OA in 2008 were used to derive the GPP, which were summed to give daily values for evaluating the performances of daily GPP simulations.

The Nash–Sutcliffe model efficiency coefficient (E) and the root mean square error (RMSE) were calculated to evaluate the model performance. E was determined following Nash and Sutcliffe (1970):

$$E = 1 - \frac{\sum_{i=1}^{N} (GPP_p - GPP_m)^2}{\sum_{i=1}^{N} (GPP_p - \overline{GPP_m})^2} \tag{16}$$

where GPP_P is the model prediction; GPP_m is the measurement; $\overline{GPP_m}$ represents the mean value of measurements; and N is the total number of data points. The E ranges from $-\infty$ to 1. The closer the E is to 1, the more accurate the model is.

Results

Evaluation of the different temporal upscaling scheme performances for daily GPP simulations

With diurnal variations of radiation, temperature, and VPD being considered, the GPP simulated using IDM closely followed the seasonal trend during the entire growing season in 2008 for both the evergreen and deciduous forest sites (Figs. 2, 3). Figure 2 shows that IDM could capture most of the day-to-day variability of GPP, except for the two periods from day 135 to 150 and from day 215 to 235 when IDM overestimates daily GPP derived from tower measurements. The R^2 values between tower-derived and simulated GPP by IDM were 0.92 with a RMSE of 1.49 g C $m^{-2}\ day^{-1}$ and an E of 0.9 for the SK-OA site and 0.87 with a RMSE of 1.77 g C $m^{-2}\ day^{-1}$ and an E of 0.83 for the BC-DF49 site. Similarly, SDM tracked the seasonal variation of GPP including the summer time peak values. At both sites, GPP by SDM matched tower-derived GPP well. For the SK-OA site, SDM explained 92 % of the daily variance of GPP with an RMSE of 1.48 g C $m^{-2}\ day^{-1}$ and an E of 0.90, whereas for BC-DF49, it explained 87 % of the daily variance of GPP with a RMSE of 2.04 g C $m^{-2}\ day^{-1}$ and an E value of 0.81. Although SADM captured most of the day-to-day variation of GPP, it tended to

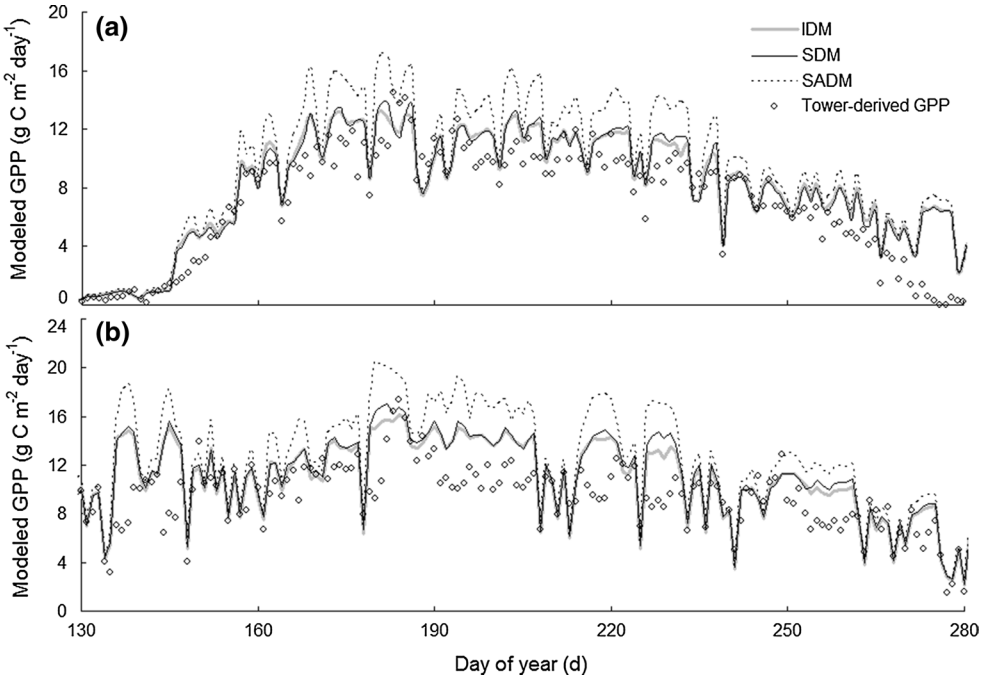

Fig. 2 Seasonal variation of tower-derived and simulated gross primary production (*GPP*) using the integrated daily model (*IDM*), the simple average daily model (*SADM*) and the segmented daily model (*SDM*) for **a** the SK-OA site and **b** the BC-DF49 site

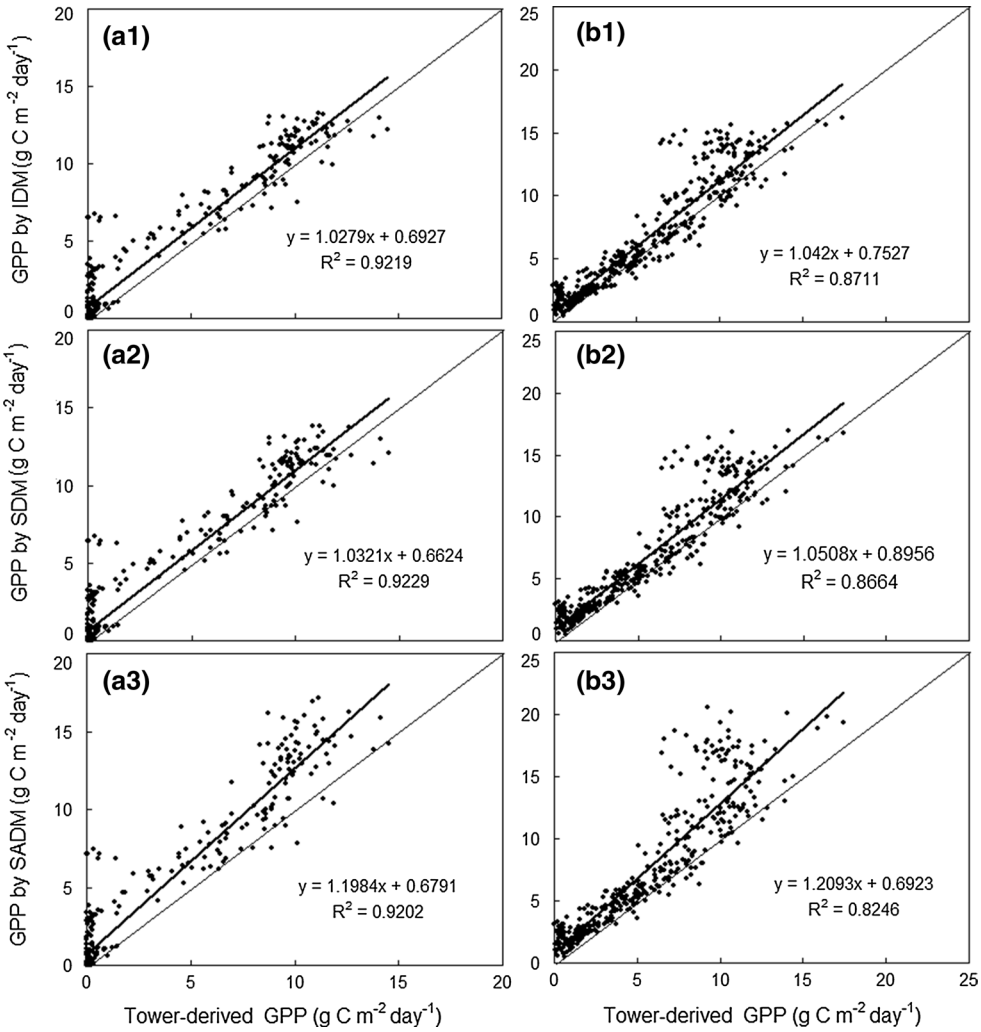

Fig. 3 Scatter plots of simulated GPP using the integrated daily model (*IDM*) (**a1**, **b1**), the segmented daily model (SDM) (**a2**, **b2**) and the simple average daily model (*SADM*) (**a3**, **b3**) versus tower-derived GPP. *Diagonal lines* are the 1:1 lines. The (**a**) panels are for SK-OA and the (**b**) panels are for BC-DF49

consistently overestimate GPP, especially for sunny summer days when global radiation was usually high. The RMSE values by SADM were 2.2 g C m^{-2} day^{-1} with an *E* value of 0.85 for SK-OA, and 2.77 g C m^{-2} day^{-1} with an *E* value of 0.71 for BC-DF49.

Comparison of different temporal upscaling schemes in GPP simulation

Overall comparison of different temporal upscaling schemes

Although IDM and SDM are different in their temporal upscaling formulations, they simulated almost the same daily GPP values in both phase and magnitude (Fig. 2). The *E* values between GPP values by IDM and SDM were 0.999 with a RMSE of 0.18 g C m^{-2} day^{-1} and 0.996 with a RMSE of 0.32 g C m^{-2} day^{-1} for SK-OA and BC-DF49, respectively. SADM behaved slightly differently than IDM and SDM, the GPP by SADM were higher than GPP by IDM and SDM, which means SADM overestimated GPP given that GPP by IDM and SDM agreed well with tower-derived GPP by taking into account the diurnal variations of photosynthesis the responses to meteorological variables. Compared to SADM, IDM improved GPP simulation by increasing the *E* value by 6 and 17 % for SK-OA and BC-DF49 and by decreasing the RMSE by 33 and 36 % for SK-OA and BC-DF49, respectively. The comparison results between SADM and SDM were similar to those with IDM (Fig. 2). Compared to SADM, SDM improved the simulation of daily GPP by increasing the *E* values by 6 and 14 % and by decreasing the RMSE by 33 and 26 % for SK-OA and BC-DF49, respectively.

Comparison of seasonal patterns of GPP by different temporal upscaling schemes

The three temporal upscaling schemes generate three pairs of comparison, i.e., IDM versus SDM, IDM versus SADM, and SDM versus SADM. Because IDM and SDM show similar GPP simulation results (Fig. 2), only the comparison between IDM and SADM is presented for the sake of brevity. At both sites, the GPP values by SADM were higher than those by IDM over the entire year (Fig. 2), indicating the overestimation by SADM simulations in which the inputs were daily total or averaged meteorological data. The absolute differences between GPP values simulated using IDM and SADM basically follow the same patterns as the seasonal variations of GPP, i.e., the larger the tower-derived GPP values in Fig. 2, the higher the absolute differences in Fig. 4. The maximum absolute differences occurred in summer, and the minimum absolute differences occurred in winter for both sites. This was also true for the

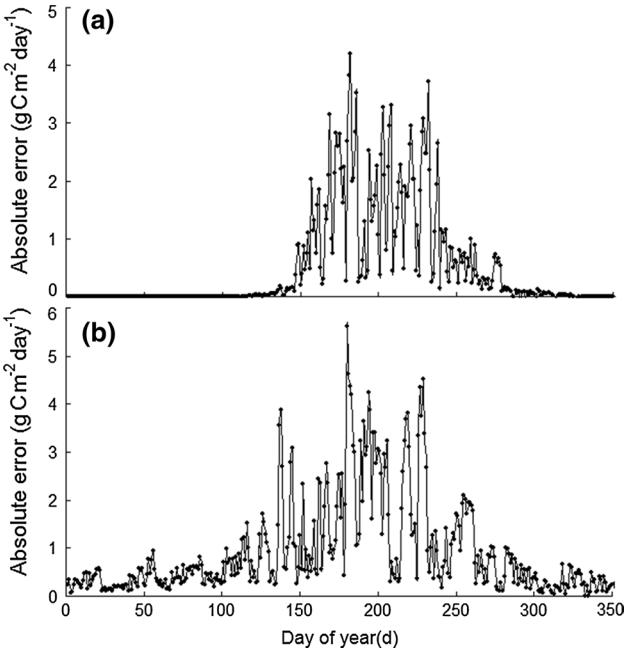

Fig. 4 Seasonal variation of the absolute differences between simulated GPP using the simple average daily model (SADM) and the integrated daily model (IDM) for **a** SK-OA site and **b** BC-DF49 site

relative difference between IDM and SADM GPP, which is because strong incident solar radiation during summer days caused saturation of canopy photosynthesis, resulting in low light use efficiency. Such summer depression in light use efficiency due to photosynthesis saturation was also observed by Goerner et al. (2009).

Comparison of computational efficiency between IDM and SDM

From the algorithms of IDM and SDM (Eqs. 5–13), it can be seen that the computational efficiency of SDM is higher than that of IDM, because numerical integration instead of the analytic solution of Eq. 5 was made to obtain daily GPP. For IDM, the hourly GPP values would in average be calculated 12 times using Eqs. 1a–1d, following a quasi-sine function, but, for SDM, the calculation of GPP using Eqs. 1a–1d is performed only twice. Therefore, in theory, SDM can decrease the computation time of IDM by 83 % in executing the code for the calculation of photosynthesis, which is the main part of the entire program. However, other parts of the program such as reading the inputs and writing the outputs also require some computational resources for both SDM and IDM, although these parts often execute once for the entire program. These parts of the program will increase the ratio of computation time of SDM to that of IDM, especially for a study site with a few pixels, but if a region with a large number of pixels is involved into the

daily GPP calculation, the computation time of SDM may approach one-sixth of that of IDM, because the input/output time may account for only a small fraction of the total computation time. In our study, since the methods of SDM and IDM were tested at two sites, SDM decreased the computation time of IDM by >66 %.

Discussion

Effects of simulated meteorological data on daily GPP

Comparing the IDM/SDM models, which are driven by simulated meteorological data, to a version of the IDM model that is driven by observed meteorological data will reveal the effects of simulated meteorological factors on daily GPP. By comparing these results, we found that there were relatively small differences between GPP by IDM/SDM driven by measured and simulated meteorological data, as shown in Fig. 5. The mean absolute relative difference (MARD) between GPP by IDM/SDM driven by measured and simulated meteorological data was 7.6/6.8 % with an E value of 0.99/0.99 for SK-OA and 6.2/7.9 % with an E value of 0.97/0.97 for BC-DF49, respectively. The similar GPP results indicated that, for most days in a given year, solar radiation, air temperature, and relative humidity (or VPD) could be accurately simulated by Eqs. 2–4, which assume that the diurnal courses of meteorological factors follow a sine function. Although obvious biases between measured and modeled VPD were observed (Online Resource 1), they had negligible effects on daily GPP simulation, as shown in Online Resources 2 and 3, because VPD with relatively low values had no significant effects on photosynthesis. However, the diurnal simulation of solar radiation did affect the simulation of daily GPP (Online Resource 4). If the sinusoidal assumption for solar radiation could not be satisfied due to the effects of precipitation and cloud formation, biases in GPP might occur in IDM and SDM simulations. The discrepancy might be partly caused by the days in which the diurnal variations of solar radiation do not perfectly follow the trajectory of a sine function, especially for those points that deviate far from the regression line (Online Resource 4).

Reasons behind the overestimation by SADM

We further explored the reason behind the overestimation caused by SADM. The daily course of solar radiation usually follows a sine function. From sunrise to noon, incident solar radiation is increasing, while light-use efficiency is decreasing and reaches its lowest at noon. When daily average radiation is used to calculate daily GPP, the radiation near solar noon (part B in Fig. 6a) will compensate for the radiation in the early morning (part A in Fig. 6a) and the magnitude of A equals that of B. Although the amount of radiation of part A is identical to that of part B, they will yield different GPP because they have different light-use efficiencies. Part B with low light-use efficiency can yield GPP shown as part B1 in Fig. 6b, but part A compensated by part B with high

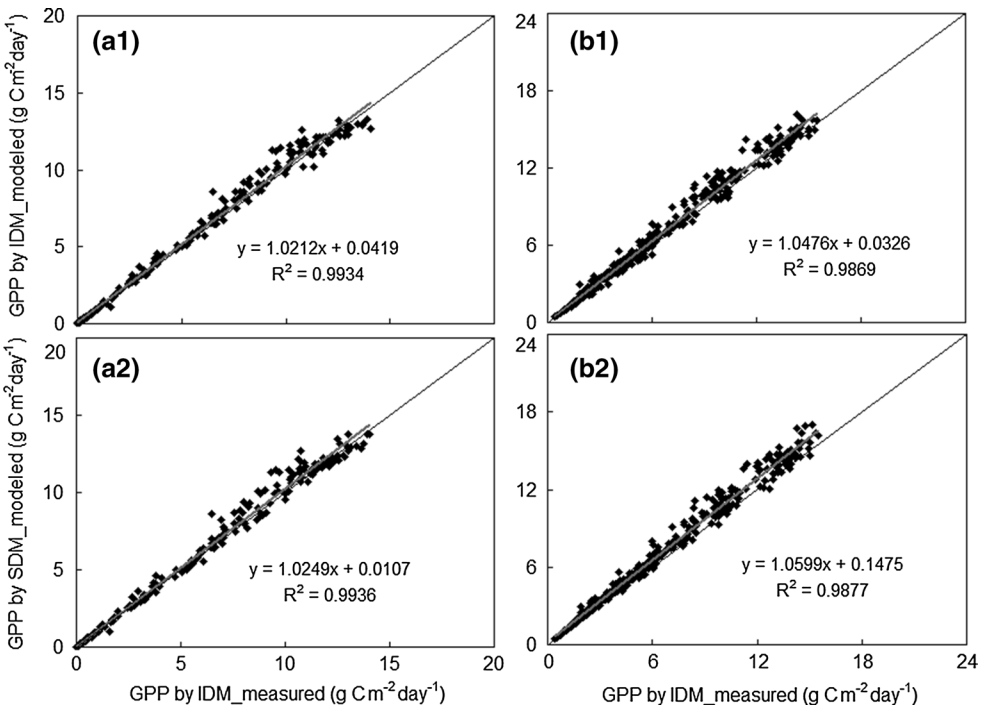

Fig. 5 Scatter plots of GPP simulated by the integrated daily model (IDM) (**a1**, **b1**) and the segmented daily model (SDM) (**a2**, **b2**) versus GPP simulated by the IDM forced by measured meteorological data. *Diagonal lines* are the 1:1 lines. The (**a**) panels are for SK-OA and the (**b**) panels are for BC-DF49

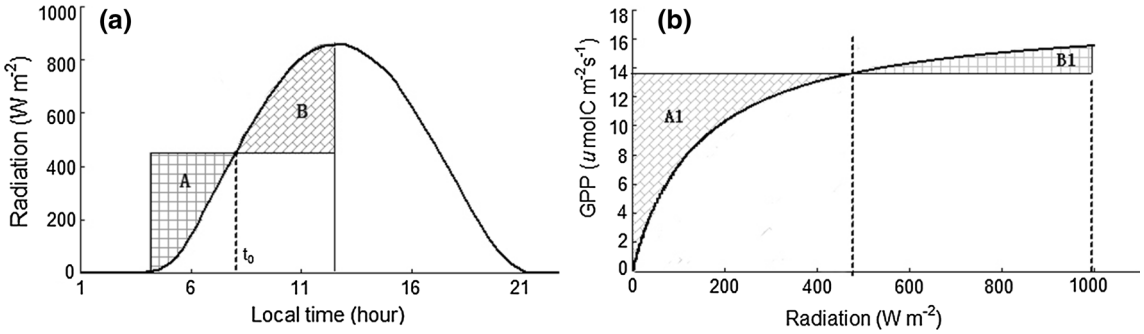

Fig. 6 Schematic diagram for **a** partitioning of daily radiation (*A* and *B*) using the simple average daily model (SADM), and **b** the corresponding net photosynthesis rate (*A1* and *B1*) from the partitioned radiation *A* and *B*. The *horizontal lines* in (**a**) and (**b**) are daily average radiation and its corresponding GPP, respectively

light-use efficiency can yield higher GPP shown as part A1 in Fig. 6b. When part B is used to compensate for part A due to the use of the daily average radiation, the light use efficiency of part B will be increased. Therefore, the total daily GPP will be overestimated. In fact, the overestimation of SADM is from the nonlinear responses of photosynthesis to environmental variables, especially to solar radiation which is highly non-linear. In addition, other environment factors such high VPD may also have an effect on the overestimation.

SADM used in this study was under the framework of a two-leaf parameterization of radiative transfer, in which sunlit leaves receive more solar radiation than shaded leaves, resulting in a greater non-linear response of GPP of sunlit leaves to solar radiation than of shaded leaves (as shown in Online Resource 5), which is consistent with the results of Bonan et al. (2012). Therefore, we can infer that most of the overestimation by SADM results from sunlit leaves.

Uncertainties and limitations of IDM and SDM simulations for daily GPP

In IDM simulation, a time lag of 2 h was taken into account, which resulted in the solar radiation and air temperature maxima occurring at different times. We compared the daily GPP simulated by considering a 2-h time lag (IDM simulation) and without time lag (IDM-NOLAG simulation). The results showed that the mean relative differences between GPP from IDM simulation and IDM-NOLAG simulation were 0.81 and 0.16 % for the growing season from May to September for SK-OA and BC-DF49, respectively. IDM-NOLAG simulation slightly increased the daily GPP estimation as a result of the increase of the temperature in the morning, but the increase had no significant effect on total daily GPP. Therefore, the effect of the time lag can be ignored in daily GPP simulation to gain computational efficiency.

In this study, three critical meteorological parameters are considered regarding the effect of their diurnal variations on GPP. But the soil water factor was not considered in IDM and SDM, which would result in an error in a water-stress environment. A possible solution to this problem is to introduce a soil water factor into the Leuning model by considering the soil water balance components. In addition, since only two sites were used in this study, IDM and SDM need to be tested at sites with large range of environmental conditions in future.

Conclusions

This study focused on temporal upscaling of photosynthesis from instantaneous to the daily time scale. Two daily canopy photosynthesis models were developed for daily photosynthesis calculations, IDM and SDM, which take diurnal variations of meteorological variables into account. IDM considers these diurnal variations using a sine function during the daytime period, while SDM alleviates the nonlinear response of photosynthesis to solar radiation by dividing daily solar radiation into two segments, and the response of photosynthesis to each segment of solar radiation could be regarded as quasi-linear. The performances of the two temporal upscaling schemes as well as SADM were compared and validated using eddy covariance CO_2 flux measurements. Both IDM and SDM can reasonably simulate both the magnitudes and day-to-day variations of GPP for two forest sites, while SADM without considering the diurnal variation of meteorological inputs overestimated the daily GPP for both sites. The overestimation mainly resulted from the use of daily total or average solar radiation which incorrectly increases the daily light use efficiency.

Comparison analysis indicated that IDM and SDM performed similarly, and better than SADM for daily canopy photosynthesis simulation, but SDM decreased the

computation time of IDM by >66 %. This result showed the promising potential of SDM for accurately simulating daily GPP with high computational efficiency, particularly for large-scale GPP simulations. In addition, a distinctive feature of IDM and SDM from some daily GPP models (Liu et al. 1997; Chen et al. 1999) is the use of a coupled photosynthesis-stomatal model, which not only strengthens the mechanism of these daily models, but also facilitates the calculations of other fluxes, such as evapotranspiration.

Acknowledgments This study is supported by the Natural Science Foundation of China (41371393, 51109183), the Specialized Research Fund for the Doctoral Program of Higher Education of China (20110101120036), and the opening foundation of Institute of Remote Sensing and Earth Sciences, Hangzhou Normal University (PDKF2011YG03). We thank the Fluxnet-Canada networks, the site principal investigators, co-investigators and participants for contributing to the flux tower datasets.

References

Baldocchi D (1994) An analytical solution for coupled leaf photosynthesis and stomatal conductance models. Tree Physiol 14:1069–1079

Ball JT (1988) An analysis of stomatal conductance. PhD thesis, Stanford University, Stanford

Barr AG, Black TA, Hogg EH, Kljun N, Morgenstern K, Nesic Z (2004) Inter-annual variability in the leaf area index of a boreal aspen-hazelnut forest in relation to net ecosystem production. Agric For Meteorol 126:237–255

Bonan GB, Oleson KW, Fisher RA, Lasslop G, Reichstein M (2012) Reconciling leaf physiological traits and canopy flux data: use of the TRY and FLUXNET databases in the community land model version 4. J Geophys Res, vol 117. doi:10.1029/2011JG001913

Chen JM, Jiu J, Cihlar J, Goulden ML (1999) Daily canopy photosynthesis model through temporal and spatial scaling for remote sensing applications. Ecol Modell 124:99–119

Chen JM, Govind A, Sonnentag O, Zhang Y, Barr A, Amiro B (2006) Leaf area index measurements at Fluxnet-Canada forest sites. Agric For Meteorol 140:257–268

Chen B, Black TA, Coops NC, Hilker T, Trofymow JA, Morgenstern K (2009) Assessing tower flux footprint climatology and scaling between remotely sensed and eddy covariance measurements. Bound Layer Meteorol 130:137–167

Farquhar GD, Von Caemmerer S, Berry JA (1980) A biochemical model of photosynthetic CO2 assimilation in leaves of C3 species. Planta 149:78–90

Goerner A, Reichstein M, Rambal S (2009) Tracking seasonal drought effects on ecosystem light use efficiency with satellite-based PRI in a Mediterranean forest. Remote Sens Environ 113:1101–1111

Groenendijk M, Dolman AJ, Ammann C, Arneth A, Cescatti A, Dragoni D, Gash JHC, Gianelle D, Gioli B, Kiely G, Knohl A, Law BE, Lund M, Marcolla B, van der Molen MK, Montagnani L, Moors E, Richardson AD, Roupsard O, Verbeeck H,and Wohlfahrt G (2011) Seasonal variation of photosynthetic model parameters and leaf area index from global Fluxnet eddy covariance data. J Geophys Res G. 116. doi:10.1029/2011JG001742

Hunt ER, Lavigne JMB, Franklin SE (1999) Factors controlling the decline of net primary production with stand age for balsam fir in Newfoundland assessed using an ecosystem simulation model. Ecol Modell 122:151–164

Izaurralde RC, Williams JR, McGill WB, Rosenberg NJ, Jakas MCQ (2006) Simulating soil C dynamics with EPIC: model description and testing against long-term data. Ecol Modell 192:362–384

Jarvis PG (1976) The interpretation of the variations in leaf water potential and stomatal conductance found in canopies in the field. Philos Trans R Soc Lond B 273:593–610

Jassal RS, Black TA, Spittlehouse DL, Brümmer C, Nesic Z (2009) Evapotranspiration and water use efficiency in different-aged Pacific Northwest Douglas-fir stands. Agric For Meteorol 149:1168–1178

Jin S, Zhou X, Fan J (2003) Modeling daily photosynthesis of nine major tree species in northeast China. For Ecol Manag 184:125–140

Kattge J, Knorr W, Raddatz T, Wirth C (2009) Quantifying photosynthetic capacity and its relationship to leaf nitrogen content for global-scale terrestrial biosphere models. Glob Change Biol 15:976–991

Katul GG, Palmroth S, Oren R (2009) Leaf stomatal responses to vapour pressure deficit under current and CO2-enriched atmosphere explained by the economics of gas exchange. Plant Cell Environ 32:968–979

Kimball BA, Bellamy LA (1986) Generation of diurnal solar radiation, temperature and humidity patterns. Energ Agr 5:185–197

Leuning R (1990) Modeling stomata1 behavior and photosynthesis of eucalyptus grandis. Aust J Plant Physiol 17:159–175

Leuning R (1995) A critical appraisal of a combined stomatal-photosynthesis model for C3 plants. Plant Cell Environ 18:1129–1146

Li C (2000) Modeling trace gas emissions from agricultural ecosystems. Nutr Cycl Agroecosyst 58:259–276

Lim WH, Roderick ML (2012) A framework for upscaling short-term process-level understanding to longer time scales. Hydrol Earth Syst Sci Discuss 9:6203–6224

Liu J, Chen JM, Cihlar J, Park WM (1997) A process-based boreal ecosystem productivity simulator using remote sensing inputs. Remote Sens Environ 62:158–175

Mäkelä A, Kolari P, Karimäki J, Nikinmaa E, Perämäki M, Hari P (2006) Modeling five years of weather-driven variation of GPP in a boreal forest. Agric For Meteorol 139:382–398

Medlyn BE, Badek FW, de Pury DGG, Barton CVM, Broadmeadow M, Ceulemans R, De Angelis P, Forstreuter M, Jach ME, Kellomäki S, Laitat E, Marek M, Philippot S, Rey A, Strassemeyer J, Laitinen K, Liozon R, Portier B, Roberntz P, Wang K, Jstbid PG (1999) Effects of elevated [CO_2] on photosynthesis in European forest species: a meta-analysis of model parameters. Plant Cell Environ 22:1475–1495

Nash JE, Sutcliffe JV (1970) River flow forecasting through conceptual models part I—a discussion of principles. J Hydrol 10:282–290

Oren R, Sperry JS, Katul GG, Pataki DE, Ewers BE, Phillips N, Schäfer KVR (1999) Survey and synthesis of intra-and interspecific variation in stomatal sensitivity to vapour pressure deficit. Plant Cell Environ 22:1515–1526

Pan Y, Birdsey R, Hom J, McCullough K (2009) Separating effects of changes in atmospheric composition, climate and land-sue on carbon sequestration of US. Mid-atlantic temperate forests. For Ecol Manag 259:151–164

Reicosky DC, Winkelman LJ, Baker JM, Baker DG (1989) Accuracy of hourly air termperatures calculated from daily minima and maxima. Agric For Meteorol 46:193–209

Running SW, Coughlan JC (1988) A general model of forest ecosystem processes for regional application. Ecol Modell 42:125–154

Sellers PJ, Berry JA, Collatz GJ, Field CB, Hall FG (1992) Canopy reflectance, photosynthesis and transpiration. III. A reanalysis using improved leaf models and a new canopy integration scheme. Remote Sens Environ 42:187–216

Thornton PE, Law BE, Gholz HL, Clark KL, Falge E, Ellsworth DS, Goldstein DS, Monson RK, Hollinger D, Falk M, Chen J, Sparks JP (2002) Modeling and measuring the effects of disturbance history and climate on carbon and water budgets in evergreen needle leaf forests. Agric For Meteorol 113:185–222

Tian H, Chen G, Liu M, Zhang C, Sun G, Lu C, Xu X, Ren W, Pan S, Chappelk A (2010) Model estimates of net primary productivity, evapotranspiration, and water use efficiency in the terrestrial ecosystems of the southern United States during 1895–2007. For Ecol Manag 259:1311–1327

Wang YP, Leuning R (1998) A two-leaf model for canopy conductance, photosynthesis and partitioning of available energy. I: model description and comparison with a multi-layered model. Agric For Meteorol 91:89–111